iScience

CellPress
OPEN ACCESS

Article

Grass carp reovirus VP56 and VP35 induce formation of viral inclusion bodies for replication

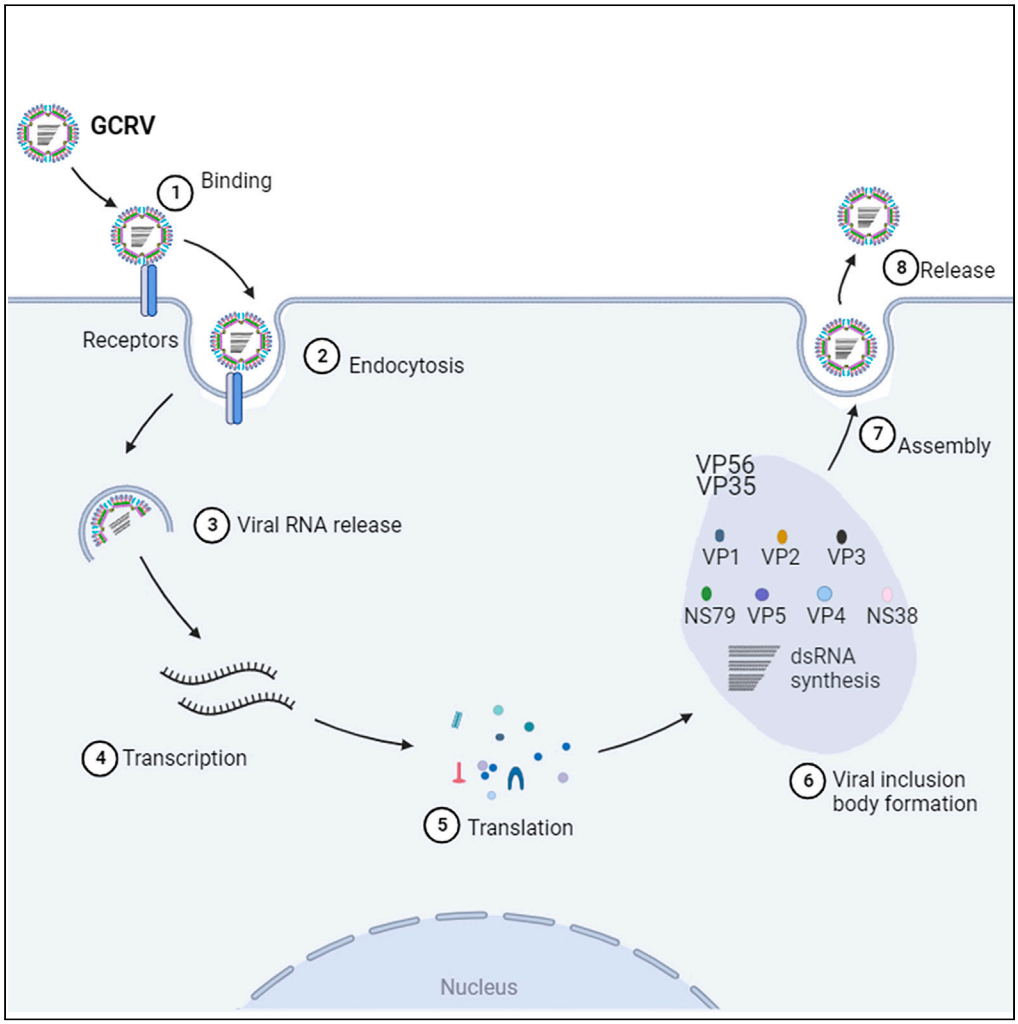

Chu Zhang, Hui Wu, Hao Feng, Yong-An Zhang, Jiagang Tu

yonganzhang@mail.hzau.edu.cn (Y.-A.Z.)
tujiagang@mail.hzau.edu.cn (J.T.)

Highlights

GCRV-II infection induces viral inclusion bodies (VIBs) formation

VP56 and VP35 induce VIBs formation

The N-terminal of VP56 and the middle domain of VP35 recruit viral proteins to VIBs

Newly synthesized viral RNAs are localized to the VIBs

Zhang et al., iScience 27, 108684
January 19, 2024
https://doi.org/10.1016/j.isci.2023.108684

iScience

CellPress
OPEN ACCESS

Article

Grass carp reovirus VP56 and VP35 induce formation of viral inclusion bodies for replication

Chu Zhang,[1] Hui Wu,[2] Hao Feng,[2] Yong-An Zhang,[1,*] and Jiagang Tu[1,3,*]

SUMMARY

Viral inclusion bodies (VIBs) are subcellular structures required for efficient viral replication. How type II grass carp reovirus (GCRV-II), the mainly prevalent strain, forms VIBs is unknown. In this study, we found that GCRV-II infection induced punctate VIBs in grass carp ovary (GCO) cells and that non-structural protein 38 (NS38) functioned as a participant in VIB formation. Furthermore, VP56 and VP35 induced VIBs and recruited other viral proteins via the N-terminal of VP56 and the middle domain of VP35. Additionally, we found that the newly synthesized viral RNAs co-localized with VP56 and VP35 in VIBs during infection. Taken together, VP56 and VP35 induce VIB formation and recruit other viral proteins and viral RNAs to the VIBs for viral replication, which helps identify new targets for developing anti-GCRV-II drugs to disrupt viral replication.

INTRODUCTION

Grass carp reovirus (GCRV), a member of the genus *Aquareovirus*, family *Reoviridae*, is a nonenveloped, icosahedral virus that contains a genome of 11 double-stranded RNA segments. The disease caused by GCRV, especially type II GCRV (GCRV-II), has resulted in huge economic losses in grass carp culture in China.[1] However, no efficient vaccines or drugs are available for GCRV-II infection. Therefore, it's urgent to understand the life cycle of GCRV-II for developing anti-viral drugs against GCRV-II infection.

A variety of viruses transcribe and replicate their genomes within specialized intracellular compartments named viral inclusion bodies (VIBs, also named viral factories, replication organelles, viral replication compartments, virosomes, or viroplasms).[2,3] This includes DNA viruses such as vaccinia virus[4] and African swine fever virus,[2] and RNA viruses such as members of the family *Togaviridae* (e.g., Sindbis virus),[5] *Nodaviridae* (e.g., flock house virus),[6] *Flaviviridae* (e.g., hepatitis C virus, HCV),[7,8] *Bunyaviridae* (e.g., rift valley fever virus),[2] *Filoviridae* (e.g., Ebola virus, EBOV),[9] *Paramyxoviridae* (e.g., measles virus, MeV),[10–12] *Reoviridae* (e.g., rotavirus),[13] *Rhabdoviridae* (e.g., vesicular stomatitis virus, VSV).[14] Recent study revealed that the nucleoprotein and phosphoprotein of MeV formed liquid-like phase-separated membraneless VIBs to promote nucleocapsid assembly.[10] Wolff et al.[15] determined the structure of coronavirus-induced VIBs and identified a molecular pore complex that spanned the membranes of the double-membrane VIBs, which allowed the export of viral RNAs to the cytosol for translation and assembly. Besides, VIBs can also prevent the activation of the host's innate immune system. Respiratory syncytial virus (RSV) sequesters NF-κB subunit P65, melanoma differentiation-associated gene 5 (MDA5), and mitochondria antiviral signaling protein (MAVS) to the VIBs to inhibit innate immune signaling.[16,17]

The formation of VSV VIBs is induced by the viral N, P, and L proteins.[14,18] Mumps virus (MuV),[19] Parainfluenza virus,[20] Nipah virus,[21] rabies virus (RABV),[22] and MeV[11] can also form VIBs that are induced mainly by the N and P proteins. The μNS protein is required to induce VIBs formation of mammalian orthoreovirus (MRV) and avian orthoreovirus (ARV).[23,24] The formation of bluetongue virus (BTV) VIBs is induced by the NS2 protein.[25] Rotavirus requires two viral proteins (NSP2 and NSP5) to induce VIBs formation.[13] VIBs serve as a platform to concentrate viral proteins and RNAs for efficient transcription and replication of viral genomes. Within VIBs formed by rotavirus, the NSP2 and NSP5 recruit several other viral proteins (VP1, VP3, VP2, VP6, and NSP2) and pre-genomic (+) ssRNAs, resulting in the proportional co-packaging into early viral particles.[26,27] MRV μNS protein recruits the σNS, μ2, and other viral proteins to the VIBs for dsRNA synthesis.[28] The inner-capsid proteins λA, λB, and μA are recruited by the ARV μNS protein to the VIBs.[29] Thus, investigation of the components of VIBs will aid in understanding the formation process of VIBs and the life cycle of viruses, which provides anti-viral drug targets.

In this study, we investigated the components and formation process of GCRV-II VIBs. The inducer of GCRV-II VIBs formation was identified as the VP56 and VP35 proteins, which formed VIBs when expressed alone and recruited several other viral proteins and viral RNAs to the VIBs.

[1]State Key Laboratory of Agricultural Microbiology, Hubei Hongshan Laboratory, Engineering Research Center of Green Development for Conventional Aquatic Biological Industry in the Yangtze River Economic Belt, Ministry of Education, College of Fisheries, Huazhong Agricultural University, Wuhan, China
[2]State Key Laboratory of Developmental Biology of Freshwater Fish, College of Life Science, Hunan Normal University, Changsha, China
[3]Lead contact
*Correspondence: yonganzhang@mail.hzau.edu.cn (Y.-A.Z.), tujiagang@mail.hzau.edu.cn (J.T.)
https://doi.org/10.1016/j.isci.2023.108684

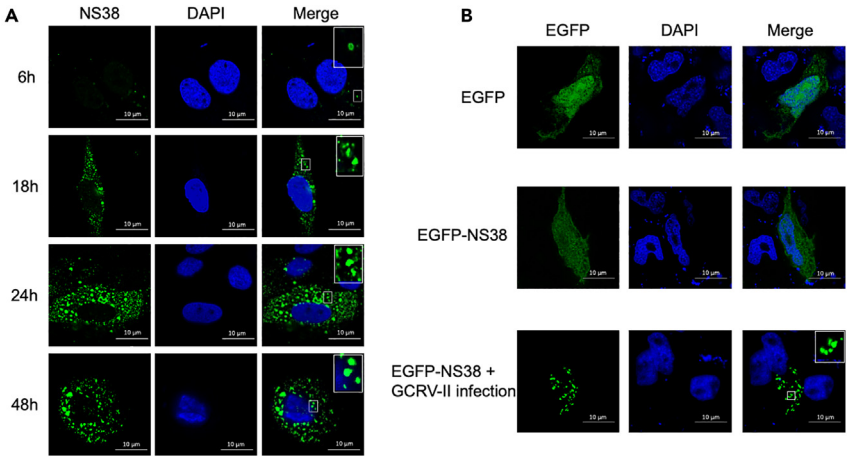

Figure 1. GCRV-II infection induces VIBs formation

(A) GCO cells were infected with GCRV-II, fixed at 6, 18, 24, and 48 hpi, and subjected to immunofluorescence using confocal microscopy with an anti-NS38 polyclonal antibody.

(B) GCO cells were transfected with pEGFP-N1 (control) or pEGFP-NS38. At 24 h post transfection, GCO cells transfected with pEGFP-NS38 were infected with or without GCRV-II. The cells were fixed and stained with DAPI. The samples were detected using confocal microscope. White squares in the upper right corner indicate the magnified area shown in the corresponding areas. Scale bar: 10 μm.

Moreover, the residues 58 to 114 at the N-terminal domain of VP56 and the residues 100 to 154 at the middle domain of VP35 were determined as the regions responsible for VIB formation. Our findings provide insights into the VIBs formation of GCRV-II for the first time, which helps to understand the life cycle of GCRV-II.

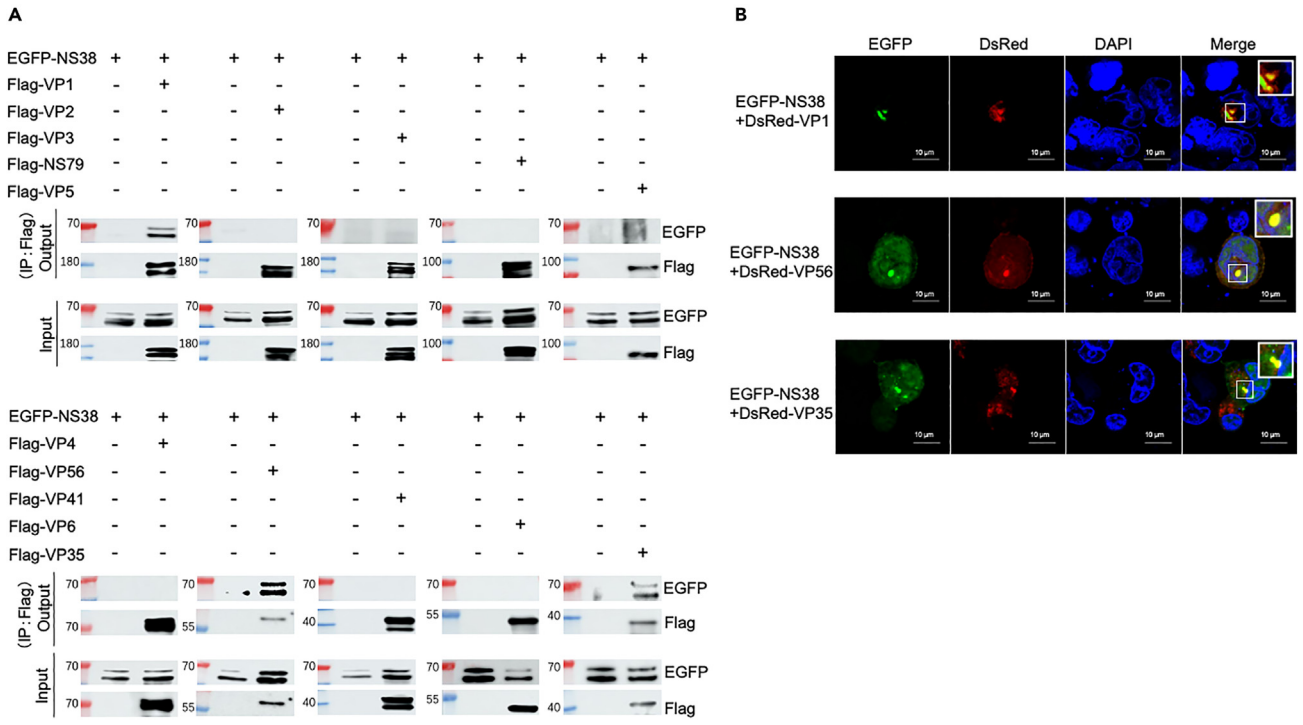

Figure 2. GCRV-II NS38 interacts with VP1, VP56, and VP35

(A) 293T cells were transfected with pEGFP-NS38, together with pFlag-VP1, pFlag-VP2, pFlag-VP3, pFlag-NS79, pFlag-VP5, pFlag-VP4, pFlag-VP56, pFlag-VP41, pFlag-VP6, pFlag-VP35, or p3XFlag-CMV-14 (control). The cells were collected at 24 h post transfection, followed by Co-IP assay with anti-Flag antibody. Then the immunoprecipitates and cell lysates were analyzed with anti-Flag and anti-EGFP antibodies.

(B) 293T cells were transfected with pEGFP-NS38, together with pDsRed-VP1, pDsRed-VP56, or pDsRed-VP35. At 24 h post transfection, the cells were fixed and stained with DAPI. The samples were detected using the confocal microscope. Scale bar: 10 μm.

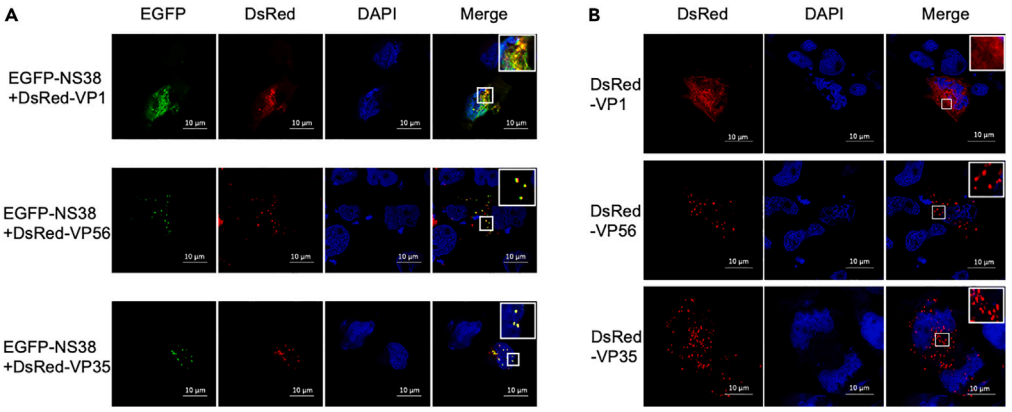

Figure 3. VP56 and VP35 induce VIBs formation

(A) GCO cells were transfected with pEGFP-NS38, together with pDsRed-VP1, pDsRed-VP56, or pDsRed-VP35. At 24 h post transfection, the cells were fixed and stained with DAPI. The samples were detected using confocal microscope.

(B) GCO cells were transfected with pDsRed-VP1, pDsRed-VP56, or pDsRed-VP35. At 24 h post transfection, the cells were fixed and stained with DAPI. The samples were detected using confocal microscope. Scale bar: 10 μm.

RESULTS

GCRV-II infection induces VIBs formation

To determine whether GCRV-II infection induces VIBs formation, GCO cells were infected with GCRV-II (strain GCRV-AH528), followed by the detection of VIBs using anti-NS38 polyclonal antibody. As shown in Figure 1A, punctate structures were observed in the cytoplasm of GCO cells. Along with the GCRV-II infection, the number of the punctate structures increased, and the diameter of the punctate structures became

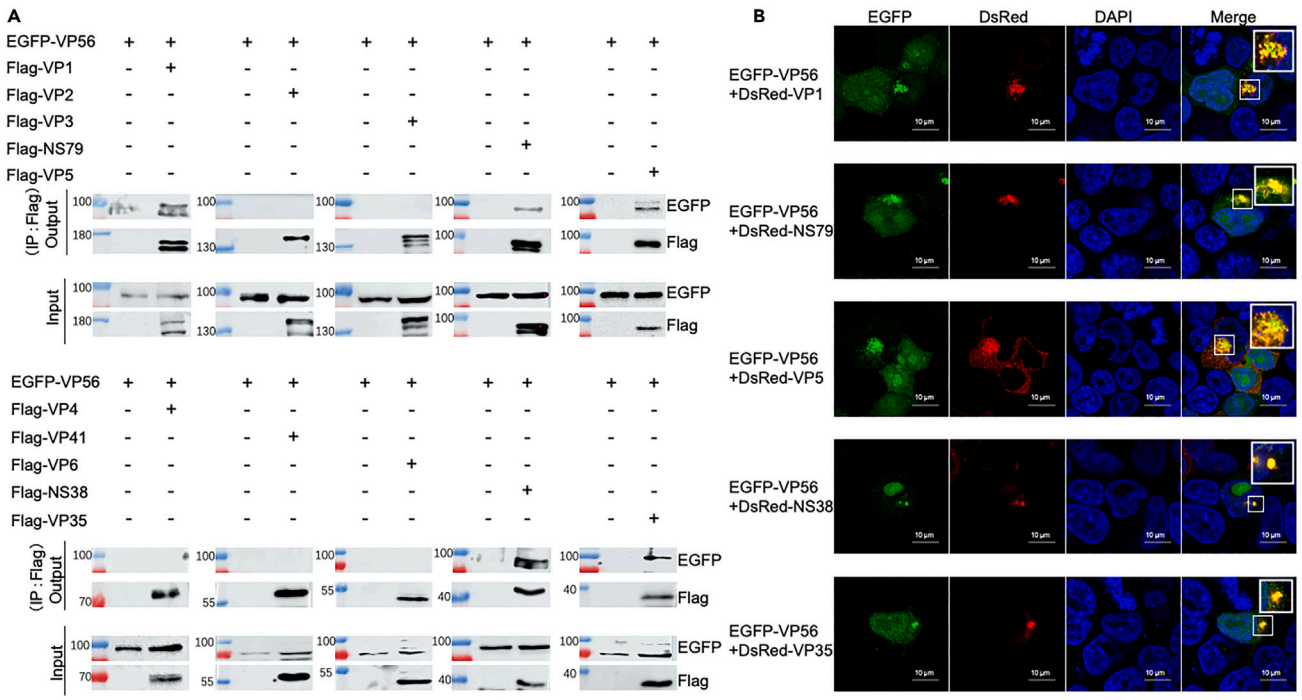

Figure 4. GCRV VP56 interacts with VP1, NS79, VP5, NS38, and VP35

(A) 293T cells were transfected with pEGFP-VP56, together with pFlag-VP1, pFlag-VP2, pFlag-VP3, pFlag-NS79, pFlag-VP5, pFlag-VP4, pFlag-VP41, pFlag-VP6, pFlag-NS38, pFlag-VP35, or p3XFlag-CMV-14(control). The cells were collected at 24 h post transfection, followed by Co-IP assay with anti-Flag antibody. Then the immunoprecipitates and cell lysates were analyzed with anti-Flag and anti-EGFP antibodies.

(B) 293T cells were transfected with pEGFP-VP56, together with pDsRed-VP1, pDsRed-NS79, pDsRed-VP5, pDsRed-NS38, or pDsRed-VP35. At 24 h post transfection, the cells were fixed and stained with DAPI. The samples were detected using confocal microscope. Scale bar: 10 μm.

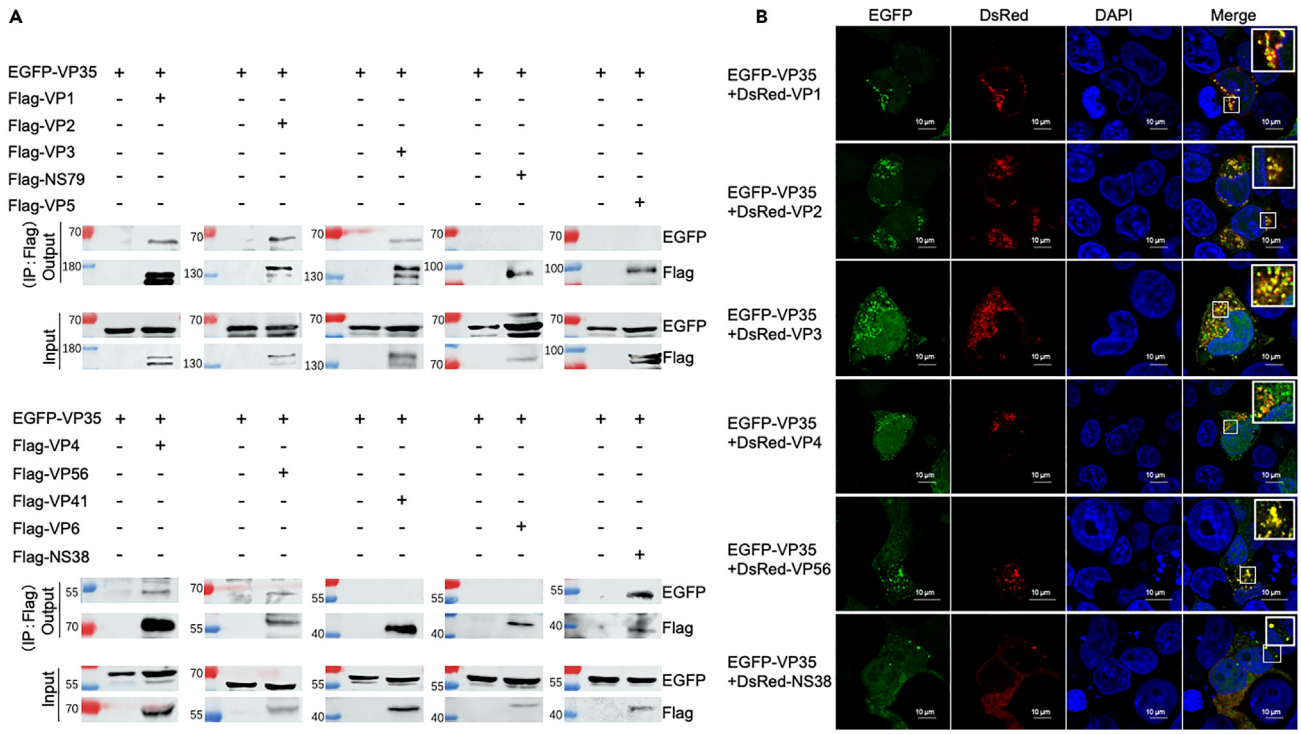

Figure 5. GCRV VP35 interacts with VP1, VP2, VP3, VP4, VP56, and NS38

(A) 293T cells were transfected with pEGFP-VP35, together with pFlag-VP1, pFlag-VP2, pFlag-VP3, pFlag-NS79, pFlag-VP5, pFlag-VP4, pFlag-VP56, pFlag-VP41, pFlag-VP6, pFlag-NS38, or p3XFlag-CMV-14(control). The cells were collected at 24 h post transfection, followed by Co-IP assay with anti-Flag antibody. Then the immunoprecipitates and cell lysates were analyzed with anti-Flag and anti-EGFP antibodies.

(B) 293T cells were transfected with pEGFP-VP35, together with pDsRed-VP1, pDsRed-VP2, pDsRed-VP3, pDsRed-VP4, pDsRed-VP56, or pDsRed-NS38. At 24 h post transfection, the cells were fixed and stained with DAPI. The samples were detected using confocal microscope. Scale bar: 10 μm.

bigger (Figure 1A). These punctate structures were similar to the VIBs observed in cells infected with MRV or aquareovirus,[13,30,31] suggesting that GCRV-II infection induced VIBs formation. To determine whether NS38 functioned as an inducer or a participant in the formation of GCRV-II VIBs, GCO cells were transfected with enhanced green fluorescent protein (EGFP) or EGFP-NS38, followed with or without GCRV-II infection. We found that NS38 was diffusely distributed in the cytoplasm of GCO cells when expressed alone but located in punctate structures under GCRV-II infection (Figure 1B), suggesting that NS38 functioned as a participant in GCRV-II VIBs formation.

VP56 and VP35 induce VIBs formation

To determine the inducer responsible for the formation of GCRV-II VIBs, 293T cells were transfected with plasmid pEGFP-NS38, together with pFlag-VP1, pFlag-VP2, pFlag-VP3, pFlag-NS79, pFlag-VP5, pFlag-VP4, pFlag-VP56, pFlag-VP41, pFlag-VP6, or pFlag-VP35. Co-immunoprecipitation assay (Co-IP) assay showed that VP1, VP56, and VP35, but not other viral proteins, interacted with NS38 (Figure 2A). Further subcellular co-localization revealed that VP1, VP56, and VP35, but not other viral proteins, co-localized with NS38 in the cytoplasm of 293T cells (Figures 2B and S1). The co-localization of NS38 with VP1, VP56, and VP35 was further investigated in GCO cells (Figure 3A). We found that NS38 was diffusely co-localized with VP1, but co-localized with VP56 and VP35 in punctate structures (Figure 3A). Furthermore, GCO cells were transfected with pDsRed-VP1, pDsRed-VP56, or pDsRed-VP35 individually. The subcellular localization of these proteins showed that VP56 and VP35, but not VP1, formed punctate structures in the cytoplasm (Figure 3B), suggesting that VP56 and VP35, but not VP1, functioned as the inducers in the formation of GCRV-II VIBs. To explore whether microtubules are involved in the formation of GCRV-II VIBs, we investigated the effects of nocodazole (Noc), a drug known to inhibit microtubule polymerization, on the morphogenesis and intracellular localization of VIBs in GCRV-II infected cells. When infected cells were treated with 10 μM nocodazole for 18 h, microtubules were completely depolymerized, but the VP56- and VP35-induced VIBs were not disrupted (Figure S2). These results indicate that the formation of GCRV-II VIBs is not dependent on a microtubule network.

VP56 and VP35 recruit viral proteins to the VIBs

To determine whether and which proteins of GCRV-II were recruited by VP56 to the VIBs, 293T cells were transfected with pEGFP-VP56, together with plasmids expressing other viral proteins. Co-IP assay showed that VP56 interacted with VP1, NS79, VP5, NS38, and VP35,

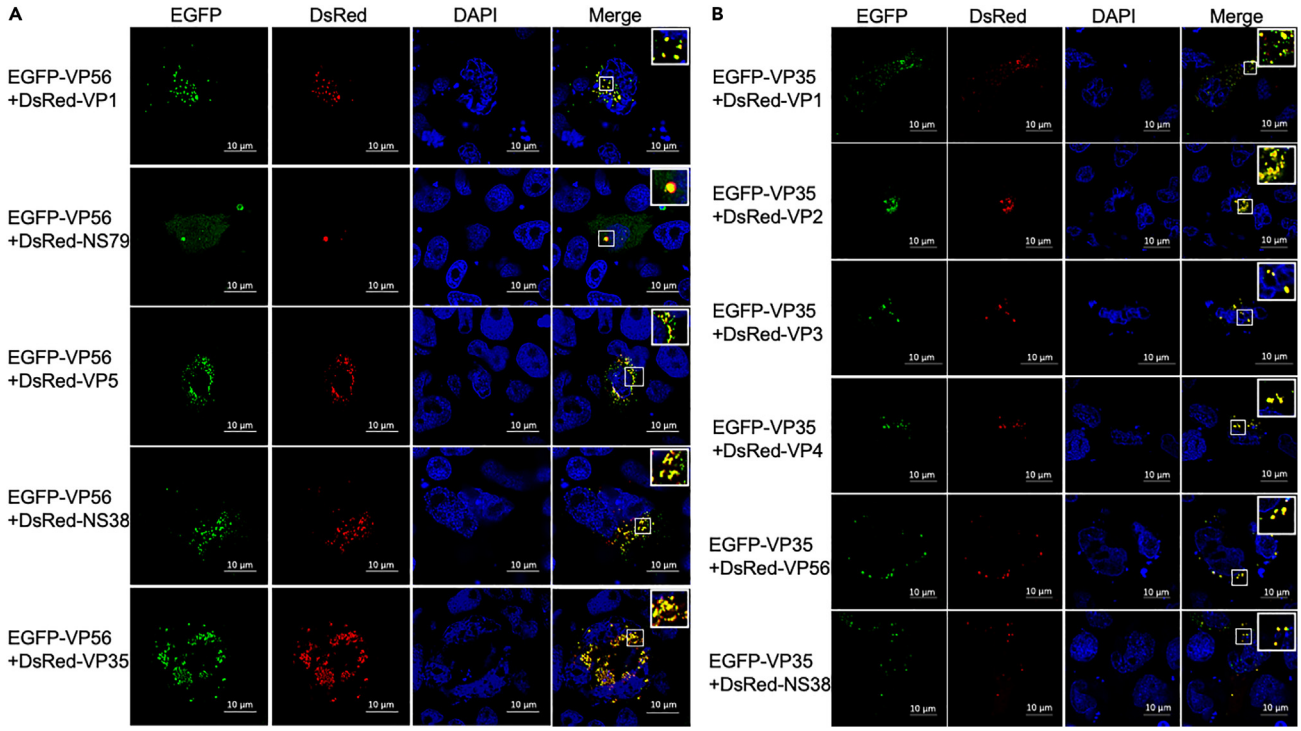

Figure 6. VP56 and VP35 recruit viral proteins to the VIBs

(A) GCO cells were transfected with pEGFP-VP56, together with pDsRed-VP1, pDsRed-NS79, pDsRed-VP5, pDsRed-NS38, or pDsRed-VP35. At 24 h post transfection, the cells were fixed and stained with DAPI. The samples were detected using confocal microscope.

(B) GCO cells were transfected with pEGFP-VP35, together with pDsRed-VP1, pDsRed-VP2, pDsRed-VP3, pDsRed-VP4, pDsRed-VP56, or pDsRed-NS38. At 24 h post transfection, the cells were fixed and counterstained with DAPI. The samples were detected using confocal microscope. Scale bar: 10 μm.

but not other viral proteins (Figure 4A). Subcellular co-localization assay demonstrated that VP1, NS79, VP5, NS38, and VP35, but not other viral proteins, co-localized with VP56 in the cytoplasm (Figures 4B and S3).

To determine whether and which proteins of GCRV-II were recruited by VP35 to the VIBs, 293T cells were transfected with pEGFP-VP35, together with plasmids expressing other viral proteins. Co-IP assay showed that VP35 interacted with VP1, VP2, VP3, VP4, VP56, and NS38, but not other viral proteins (Figure 5A). Subcellular co-localization assay demonstrated that VP1, VP2, VP3, VP4, VP56, and NS38, but not other viral proteins, were co-localized with VP35 in the cytoplasm (Figures 5B and S4).

To further confirm whether VP56 and VP35 recruited the above indicated viral proteins to the VIBs, GCO cells were transfected with plasmid pEGFP-VP56 or pEGFP-VP35, together with plasmids expressing their interacted viral proteins. We found that VP56 and VP35 co-localized with the above indicated viral proteins in punctate structures in GCO cells (Figure 6). These data suggest that VP56 and VP35 recruit several viral proteins to the VIBs.

N-terminal domain of VP56 is responsible for the VIBs formation and interaction with the recruited viral proteins

To identify which domain of VP56 is responsible for the VIBs formation, a series of VP56 truncated mutant plasmids expressing VP56-N (N-terminal domain of VP56, aa 1 to 171), VP56-M (Middle domain of VP56, aa 172 to 373), or VP56-C (C-terminal domain of VP56, aa 374 to 512) were constructed (Figure 7A). Subcellular localization revealed that VP56-N, but not VP56-M or VP56-C, formed VIBs (Figure 7B). Moreover, Co-IP assay revealed that VP56-N not only interacted with itself, but also interacted with VP1, NS79, VP5, NS38, and VP35, similar to the full-length VP56 (Figure 7C). Furthermore, to identify more precise residues of VP56-N that are necessary for the VIBs formation, the N-terminal domain of VP56 was divided into VP56-$N_{1\text{-}57}$, VP56-$N_{58\text{-}114}$, and VP56-$N_{115\text{-}171}$ (Figure S5A), based on functional region analysis by SMART software.[32] Subcellular localization revealed that VP56-$N_{58\text{-}114}$, but not VP56-$N_{1\text{-}57}$ or VP56-$N_{115\text{-}171}$, formed VIBs (Figure S5B). In addition, subcellular co-localization assay showed that VP56-$N_{1\text{-}57}$ co-localized with VP1, NS79, VP5, and NS38, but not VP35 (Figure S6A), while VP56-$N_{58\text{-}114}$ only co-localized with NS38 (Figure S6B). In contrast, VP56-$N_{115\text{-}171}$ co-localized with VP1, NS79, VP5, NS38, and VP35, similar to that of VP56-N (Figure S6C). These data suggest that the N-terminal domain of VP56 is responsible for the VIBs formation and interaction with the recruited viral proteins.

Middle domain of VP35 is responsible for the VIBs formation and interaction with the recruited viral proteins

To determine the critical domain of VP35 responsible for the formation of VIBs, a series of VP35 truncated mutant plasmids expressing VP35-N (N-terminal domain of VP35, aa 1 to 99), VP35-M (Middle domain of VP35, aa 100 to 208), or VP35-C (C-terminal domain of

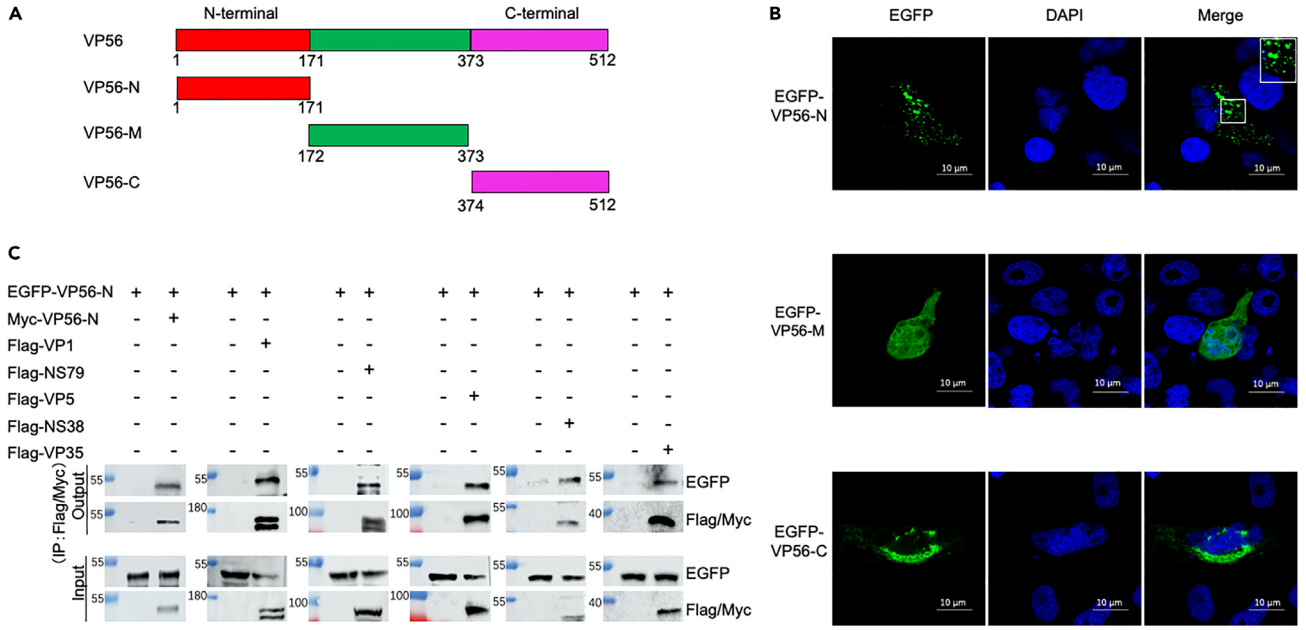

Figure 7. N-terminal domain of VP56 is responsible for the VIBs formation and interaction with the recruited viral proteins

(A) The schematic shows the plasmids expressing different VP56 truncated mutants.

(B) GCO cells were transfected with pEGFP-VP56-N, pEGFP-VP56-M, or pEGFP-VP56-C. At 24 h post transfection, the cells were fixed and stained with DAPI. The samples were detected using confocal microscope. Scale bar: 10 μm.

(C) 293T cells were transfected with pEGFP-VP56-N, together with pMyc-VP56-N, pFlag-VP1, pFlag-NS79, pFlag-VP5, pFlag-NS38, or pFlag-VP35. The cells were collected at 24 h post transfection, followed by Co-IP assay with anti-Myc or anti-Flag antibody. Then the immunoprecipitates and cell lysates were analyzed with anti-EGFP, anti-Myc, and anti-Flag antibodies.

VP35, aa 209 to 310) were constructed (Figure 8A). Subcellular localization revealed that VP35-M, but not VP35-N or VP35-C, formed VIBs (Figure 8B). Further Co-IP assay revealed that VP35-M not only interacted with itself, but also interacted with VP1, VP2, VP3, VP4, VP56, and NS38 (Figure 8C). Furthermore, to identify more precise residues of VP35-M that are necessary for VIBs formation, the middle domain of VP35 was divided into VP35-$M_{100\text{-}154}$ and VP35-$M_{155\text{-}208}$ (Figure S7A), based on functional region analysis by SMART software.[32] Subcellular localization revealed that VP35-$M_{100\text{-}154}$, but not VP35-$M_{155\text{-}208}$, formed VIBs (Figure S7B). In addition, subcellular co-localization assay showed that VP35-$M_{100\text{-}154}$ co-localized with VP1, VP2, VP3, VP56, and NS38, but not VP4 (Figure S8A), while VP35-$M_{155\text{-}208}$ co-localized with VP1, VP56, and NS38 (Figure S8B). These data suggest that the middle domain of VP35 is responsible for the VIBs formation and interaction with the recruited viral proteins.

Newly synthesized viral RNAs are localized to the VIBs in infected GCO cells

Previous findings have shown that newly synthesized viral RNAs by MRV and aquareoviruses were localized in VIBs.[33–35] To determine whether newly synthesized viral RNAs are localized in VIBs in GCRV-II infected cells, GCO cells were infected with GCRV-II. At 15 hpi, the cells were treated with actinomycin D (ActD) for 30 min to prevent cellular transcription, followed by the addition of bromouridine (BrU) for 1 h to label the newly synthesized viral RNAs. Under these conditions, the newly synthesized viral RNAs containing BrU can be visualized by BrU antibody.[36] We found that no BrU-labeled RNAs were visualized in mock-infected cells in presence of ActD, while BrU-labeled RNAs were localized in the nucleus in mock-infected cells in the absence of ActD (Figure 9A). The newly synthesized viral RNAs were co-localized in VIBs with VP56 and VP35 in GCRV-II infected cells (Figure 9B). These data suggest newly synthesized viral RNAs are localized to the VIBs in GCRV-II infected GCO cells.

DISCUSSION

Grass carp hemorrhagic disease caused by GCRV-II infection led to high morbidity and mortality in grass carp aquaculture in China. However, the life cycle of GCRV-II, especially the formation of VIBs, has rarely been investigated. In this study, we determined that GCRV-II infection induced punctate VIBs in the cytoplasm with similar morphology to those of MRV,[23] ARV,[24] and GCRV-I.[30] Moreover, we identified that VP56 and VP35, as inducers of GCRV-II VIBs, recruited other viral proteins and viral RNAs to the VIBs for viral replication. In addition, the amino acid residues 58 to 114 at the N-terminal domain of VP56 and the residues 100 to 154 at the middle domain of VP35 were identified as the regions responsible for VIBs formation. Our findings provide insights into GCRV-II VIBs formation and contribute targets for designing antiviral drugs against GCRV-II infection.

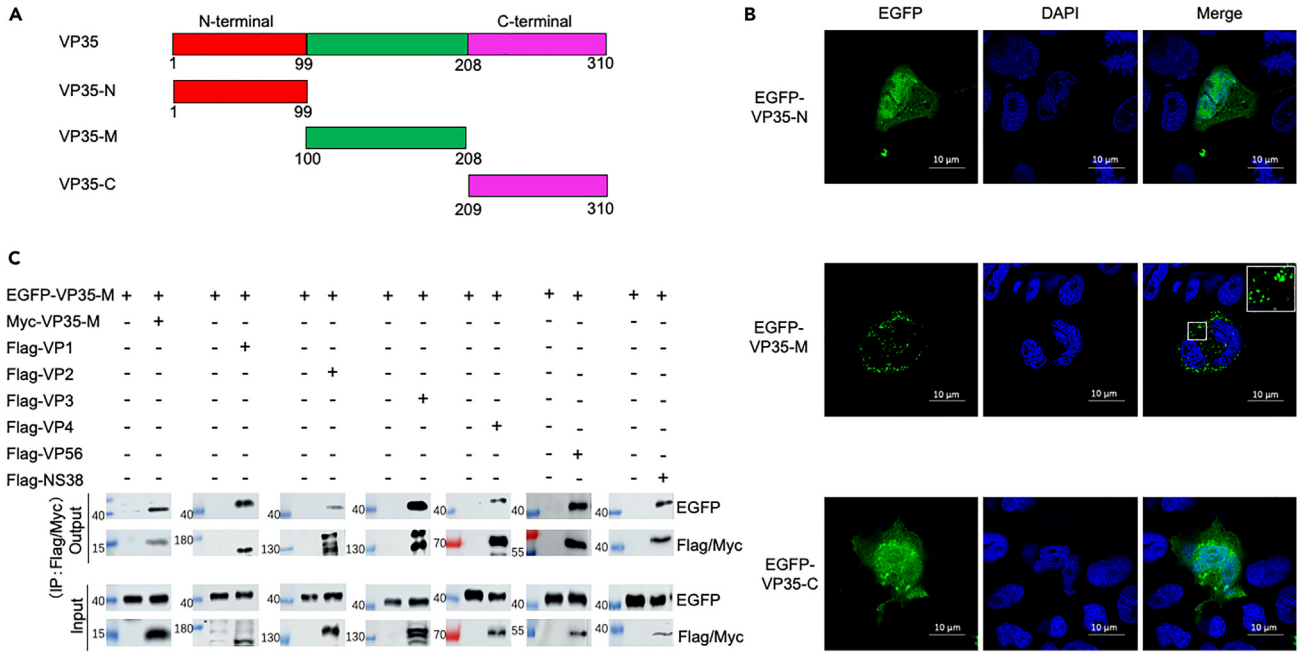

Figure 8. Middle domain of VP35 is responsible for the VIBs formation and interaction with the recruited viral proteins

(A) The schematic shows the plasmids expressing different VP35 truncated mutants.

(B) GCO cells were transfected with pEGFP-VP35-N, pEGFP-VP35-M, or pEGFP-VP35-C. At 24 h post transfection, the cells were fixed and stained with DAPI. The samples were detected using confocal microscope. Scale bar: 10 μm.

(C) 293T cells were transfected with pEGFP-VP35-M, together with pMyc-VP35-M, pFlag-VP1, pFlag-VP2, pFlag-VP3, pFlag-VP4, pFlag-VP56, or pFlag-NS38. The cells were collected at 24 h post transfection, followed by Co-IP assay with anti-Myc or anti-Flag antibody. Then the immunoprecipitates and cell lysates were analyzed with anti-EGFP, anti-Myc, and anti-Flag antibodies.

Many single-stranded negative-sense RNA viruses, including RABV,[37] EBOV,[9,38] RSV,[39,40] and MeV,[11] have been reported to initiate VIBs formation by viral N and P proteins. Double-stranded RNA viruses from the family *Reoviridae* can also initiate VIBs formation by viral proteins. The non-structural protein μNS of MRV and ARV induced punctate VIBs formation.[24,28,41] The NS80 of GCRV-I (analogue of MRV μNS), when expressed alone in cells, induced VIBs formation similar to those in GCRV-I-infected cells.[30] In our study, VP56 and VP35, when expressed alone in cells, induced VIBs formation, consistent with the findings of MRV μNS and GCRV-I NS80, indicating that these viral proteins were the inducers in the formation of VIBs.[24,30,31] However, NS79 of GCRV-II, analogue of the MRV μNS and GCRV-I NS80,[42] was localized in VIBs when co-expressed with VP56, but not when expressed alone (data not shown), indicating that GCRV-II NS79 was a participant, but not an inducer, in the formation of VIBs. Moreover, different from MRV μNS, BTV NS2, and phytoreovirus Pns12, a single viral protein induced VIBs formation,[25,31,43] GCRV-II used two viral proteins VP56 and VP35 to induce the VIBs formation, which was similar to rotavirus that required both NSP2 and NSP5 to induce VIBs formation.[13] However, whether VP56 and VP35 induced VIBs formation individually or together during GCRV-II infection needs to be further investigated.

Reoviruses utilized the inducers to recruit other viral proteins to the VIBs. Accumulating evidence suggests that the μNS protein of MRV recruits the μ2 protein to the VIBs to control the morphology and location of the VIBs, the σNS protein to the VIBs for RNA-binding, and viral core surface proteins (λ1, λ2, and σ2) to the VIBs for assembling progeny virions.[31,44] The μNS protein of ARV recruits the σNS protein to the VIBs for viral replication and assembly.[24] The two major core proteins VP7 (surface core protein) and VP3 (inner core protein) were recruited by NS2 protein of BTV to the VIBs.[25] The GCRV-I NS80 protein could recruit NS38 and VP4 to the VIBs.[45] Similar to these reports, we found that several viral proteins were recruited by VP56 and VP35 to the VIBs. Because of the differences in the localization of participants in the presence and absence of inducers, we speculate that protein interactions between inducers and participants may be a critical early step in establishing the occurrence of viral genome replication and assembly. To our knowledge, this is the first time to report VIBs formation of GCRV-II and identify the inducers and participants of the VIBs.

The VIBs of RNA viruses are usually the site for RNA synthesis.[46] Several studies have demonstrated that newly synthesized RNAs were detected in VIBs, including positive-stranded RNA viruses (flock house virus)[47] and negative-stranded RNA viruses (RSV, RABV, and EBOV).[9,39,48] In this study, we found that GCRV-II RNAs were localized to the VIBs during GCRV-II infection. The location of newly synthesized viral RNAs within VIBs has also been reported previously in reoviruses including MRV,[34] GCRV-I,[33] rotavirus,[49] and phytoreovirus.[43] Our data and previous studies suggest that initiators of the viruses in the family *Reoviridae* induce VIBs formation to provide a platform to recruit viral RNAs for RNA synthesis.

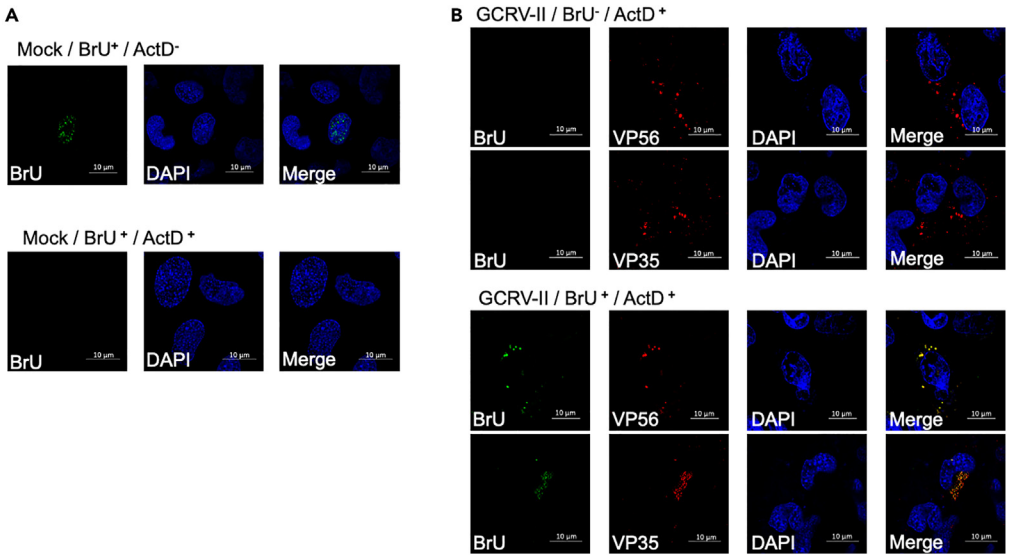

Figure 9. Newly synthesized viral RNAs are localized to the VIBs in GCRV-II infected GCO cells

(A) GCO cells were transfected with BrUTP after treatment with or without ActD for 30 min. At 1 h post transfection, the cells were fixed and stained with an anti-BrU antibody.

(B) At 15 h post of GCRV-II infection, the cells were treated with ActD for 30 min and then transfected with or without BrUTP in presence of ActD for 1 h, followed by staining with anti-BrU antibody and polyclonal antibodies against VP56 and VP35. DAPI staining was applied to detect the cell nucleus. Scale bar: 10 μm.

In conclusion, this study identified that VP56 and VP35 were the inducers of GCRV-II VIBs formation and recruited other viral proteins and viral RNAs to VIBs. Besides, the N-terminal domain of VP56 and the middle domain of VP35 were determined as the regions responsible for interacting with the recruited viral proteins and VIBs formation. Our results provide novel insights into the function of VP56 and VP35 of GCRV-II and help understand the VIBs formation of reoviruses.

Limitations of the study

A limitation of this study is that we only resolved the viral components of VIBs formation and did not investigate the host proteins involved in the formation process.

STAR★METHODS

Detailed methods are provided in the online version of this paper and include the following:

- KEY RESOURCES TABLE
- RESOURCE AVAILABILITY
  - Lead contact
  - Materials availability
  - Data and code availability
- EXPERIMENTAL MODEL AND STUDY PARTICIPANT DETAILS
  - Cells
- METHOD DETAILS
  - Plasmid construction
  - Virus infection
  - Immunoprecipitation (IP) and Western blotting
  - Immunofluorescence and confocal microscope
  - BrUTP labeling of viral RNAs
- QUANTIFICATION AND STATISTICAL ANALYSIS

SUPPLEMENTAL INFORMATION

Supplemental information can be found online at https://doi.org/10.1016/j.isci.2023.108684.

ACKNOWLEDGMENTS

This work was supported by the National Natural Science Foundation of China (31930114, 31972832, 32173014).

AUTHOR CONTRIBUTIONS

J.T. – Conceptualization, Methodology, Writing - Reviewing and Editing, Funding acquisition. Y.-A.Z. – Supervision, Writing – Reviewing and Editing, Funding acquisition. C.Z. – Data Curation, Visualization, Formal analysis, Writing – Original draft preparation. H.W. – Data Curation. H.F. – Data Curation.

DECLARATION OF INTERESTS

The authors declare no competing interests.

Received: August 23, 2023
Revised: November 14, 2023
Accepted: December 5, 2023
Published: December 7, 2023

REFERENCES

1. Su, H., and Su, J. (2018). Cyprinid viral diseases and vaccine development. Fish Shellfish Immun *83*, 84–95.
2. Novoa, R.R., Calderita, G., Arranz, R., Fontana, J., Granzow, H., and Risco, C. (2005). Virus factories: associations of cell organelles for viral replication and morphogenesis. Biol. Cell *97*, 147–172.
3. Netherton, C.L., and Wileman, T. (2011). Virus factories, double membrane vesicles and viroplasm generated in animal cells. Curr. Opin. Virol. *1*, 381–387.
4. Tolonen, N., Doglio, L., Schleich, S., and Krijnse Locker, J. (2001). Vaccinia virus DNA replication occurs in endoplasmic reticulum-enclosed cytoplasmic mini-nuclei. Mol. Biol. Cell *12*, 2031–2046.
5. Zhang, W., Mukhopadhyay, S., Pletnev, S.V., Baker, T.S., Kuhn, R.J., and Rossmann, M.G. (2002). Placement of the structural proteins in Sindbis virus. J. Virol. *76*, 11645–11658.
6. Short, J.R., Speir, J.A., Gopal, R., Pankratz, L.M., Lanman, J., and Schneemann, A. (2016). Role of Mitochondrial Membrane Spherules in Flock House Virus Replication. J. Virol. *90*, 3676–3683.
7. Romero-Brey, I., Merz, A., Chiramel, A., Lee, J.Y., Chlanda, P., Haselman, U., Santarella-Mellwig, R., Habermann, A., Hoppe, S., Kallis, S., et al. (2012). Three-dimensional architecture and biogenesis of membrane structures associated with hepatitis C virus replication. PLoS Pathog. *8*, e1003056.
8. Romero-Brey, I., Berger, C., Kallis, S., Kolovou, A., Paul, D., Lohmann, V., and Bartenschlager, R. (2015). NS5A Domain 1 and Polyprotein Cleavage Kinetics Are Critical for Induction of Double-Membrane Vesicles Associated with Hepatitis C Virus Replication. mBio *6*, e00759.
9. Hoenen, T., Shabman, R.S., Groseth, A., Herwig, A., Weber, M., Schudt, G., Dolnik, O., Basler, C.F., Becker, S., and Feldmann, H. (2012). Inclusion bodies are a site of ebolavirus replication. J. Virol. *86*, 11779–11788.
10. Guseva, S., Milles, S., Jensen, M.R., Salvi, N., Kleman, J.P., Maurin, D., Ruigrok, R.W.H., and Blackledge, M. (2020). Measles virus nucleo- and phosphoproteins form liquid-like phase-separated compartments that promote nucleocapsid assembly. Sci. Adv. *6*, eaaz7095.
11. Zhou, Y., Su, J.M., Samuel, C.E., and Ma, D. (2019). Measles Virus Forms Inclusion Bodies with Properties of Liquid Organelles. J. Virol. *93*, e00948-19.
12. Boggs, K.B., Edmonds, K., Cifuentes-Munoz, N., El Najjar, F., Ossandón, C., Roe, M., Wu, C., Moncman, C.L., Creamer, T.P., Amarasinghe, G.K., et al. (2022). Human Metapneumovirus Phosphoprotein Independently Drives Phase Separation and Recruits Nucleoprotein to Liquid-Like Bodies. mBio *13*, e0109922.
13. Fabbretti, E., Afrikanova, I., Vascotto, F., and Burrone, O.R. (1999). Two non-structural rotavirus proteins, NSP2 and NSP5, form viroplasm-like structures in vivo. J. Gen. Virol. *80*, 333–339.
14. Heinrich, B.S., Maliga, Z., Stein, D.A., Hyman, A.A., and Whelan, S.P.J. (2018). Phase Transitions Drive the Formation of Vesicular Stomatitis Virus Replication Compartments. mBio *9*, e02290-17.
15. Wolff, G., Limpens, R.W.A.L., Zevenhoven-Dobbe, J.C., Laugks, U., Zheng, S., de Jong, A.W.M., Koning, R.I., Agard, D.A., Grünewald, K., Koster, A.J., et al. (2020). A molecular pore spans the double membrane of the coronavirus replication organelle. Science *369*, 1395–1398.
16. Jobe, F., Simpson, J., Hawes, P., Guzman, E., and Bailey, D. (2020). Respiratory Syncytial Virus Sequesters NF-κB Subunit p65 to Cytoplasmic Inclusion Bodies To Inhibit Innate Immune Signaling. J. Virol. *94*, e01380-20.
17. Lifland, A.W., Jung, J., Alonas, E., Zurla, C., Crowe, J.E., Jr., and Santangelo, P.J. (2012). Human respiratory syncytial virus nucleoprotein and inclusion bodies antagonize the innate immune response mediated by MDA5 and MAVS. J. Virol. *86*, 8245–8258.
18. Heinrich, B.S., Cureton, D.K., Rahmeh, A.A., and Whelan, S.P.J. (2010). Protein expression redirects vesicular stomatitis virus RNA synthesis to cytoplasmic inclusions. PLoS Pathog. *6*, e1000958.
19. Katoh, H., Kubota, T., Kita, S., Nakatsu, Y., Aoki, N., Mori, Y., Maenaka, K., Takeda, M., and Kidokoro, M. (2015). Heat shock protein 70 regulates degradation of the mumps virus phosphoprotein via the ubiquitin-proteasome pathway. J. Virol. *89*, 3188–3199.
20. Zhang, S., Jiang, Y., Cheng, Q., Zhong, Y., Qin, Y., and Chen, M. (2017). Inclusion Body Fusion of Human Parainfluenza Virus Type 3 Regulated by Acetylated α-Tubulin Enhances Viral Replication. J. Virol. *91*, e01802-16.
21. Ringel, M., Heiner, A., Behner, L., Halwe, S., Sauerhering, L., Becker, N., Dietzel, E., Sawatsky, B., Kolesnikova, L., and Maisner, A. (2019). Nipah virus induces two inclusion body populations: Identification of novel inclusions at the plasma membrane. PLoS Pathog. *15*, e1007733.
22. Nevers, Q., Scrima, N., Glon, D., Le Bars, R., Decombe, A., Garnier, N., Ouldali, M., Lagaudrière-Gesbert, C., Blondel, D., Albertini, A., and Gaudin, Y. (2022). Properties of rabies virus phosphoprotein and nucleoprotein biocondensates formed in vitro and in cellulo. PLoS Pathog. *18*, e1011022.
23. Becker, M.M., Peters, T.R., and Dermody, T.S. (2003). Reovirus sigma NS and mu NS proteins form cytoplasmic inclusion structures in the absence of viral infection. J. Virol. *77*, 5948–5963.
24. Touris-Otero, F., Martínez-Costas, J., Vakharia, V.N., and Benavente, J. (2004). Avian reovirus nonstructural protein microNS forms viroplasm-like inclusions and recruits protein sigmaNS to these structures. Virology *319*, 94–106.
25. Kar, A.K., Bhattacharya, B., and Roy, P. (2007). Bluetongue virus RNA binding protein NS2 is a modulator of viral replication and assembly. BMC Mol. Biol. *8*, 4.
26. Trask, S.D., McDonald, S.M., and Patton, J.T. (2012). Structural insights into the coupling of virion assembly and rotavirus replication. Nat. Rev. Microbiol. *10*, 165–177.
27. Papa, G., Borodavka, A., and Desselberger, U. (2021). Viroplasms: Assembly and Functions of Rotavirus Replication Factories. Viruses *13*, 1349.
28. Becker, M.M., Goral, M.I., Hazelton, P.R., Baer, G.S., Rodgers, S.E., Brown, E.G., Coombs, K.M., and Dermody, T.S. (2001). Reovirus sigmaNS protein is required for nucleation of viral assembly complexes and formation of viral inclusions. J. Virol. *75*, 1459–1475.
29. Tourís-Otero, F., Cortez-San Martín, M., Martínez-Costas, J., and Benavente, J. (2004). Avian reovirus morphogenesis occurs within

viral factories and begins with the selective recruitment of sigmaNS and lambdaA to microNS inclusions. J. Mol. Biol. *341*, 361–374.
30. Shao, L., Guo, H., Yan, L.M., Liu, H., and Fang, Q. (2013). Aquareovirus NS80 recruits viral proteins to its inclusions, and its C-terminal domain is the primary driving force for viral inclusion formation. PLoS One *8*, e55334.
31. Broering, T.J., Parker, J.S.L., Joyce, P.L., Kim, J., and Nibert, M.L. (2002). Mammalian reovirus nonstructural protein microNS forms large inclusions and colocalizes with reovirus microtubule-associated protein micro2 in transfected cells. J. Virol. *76*, 8285–8297.
32. Letunic, I., and Bork, P. (2018). 20 years of the SMART protein domain annotation resource. Nucleic Acids Res. *46*, D493–D496.
33. Yan, L., Zhang, J., Guo, H., Yan, S., Chen, Q., Zhang, F., and Fang, Q. (2015). Aquareovirus NS80 Initiates Efficient Viral Replication by Retaining Core Proteins within Replication-Associated Viral Inclusion Bodies. PLoS One *10*, e0126127.
34. Miller, C.L., Arnold, M.M., Broering, T.J., Hastings, C.E., and Nibert, M.L. (2010). Localization of mammalian orthoreovirus proteins to cytoplasmic factory-like structures via nonoverlapping regions of microNS. J. Virol. *84*, 867–882.
35. Lee, C.H., Raghunathan, K., Taylor, G.M., French, A.J., Tenorio, R., Fernández de Castro, I., Risco, C., Parker, J.S.L., and Dermody, T.S. (2021). Reovirus Nonstructural Protein σNS Recruits Viral RNA to Replication Organelles. mBio *12*, e0140821.
36. Das, S.C., Nayak, D., Zhou, Y., and Pattnaik, A.K. (2006). Visualization of intracellular transport of vesicular stomatitis virus nucleocapsids in living cells. J. Virol. *80*, 6368–6377.
37. Nikolic, J., Le Bars, R., Lama, Z., Scrima, N., Lagaudrière-Gesbert, C., Gaudin, Y., and Blondel, D. (2017). Negri bodies are viral factories with properties of liquid organelles. Nat. Commun. *8*, 58.
38. Nanbo, A., Watanabe, S., Halfmann, P., and Kawaoka, Y. (2013). The spatio-temporal distribution dynamics of Ebola virus proteins and RNA in infected cells. Sci. Rep. *3*, 1206.
39. Rincheval, V., Lelek, M., Gault, E., Bouillier, C., Sitterlin, D., Blouquit-Laye, S., Galloux, M., Zimmer, C., Eleouet, J.F., and Rameix-Welti, M.A. (2017). Functional organization of cytoplasmic inclusion bodies in cells infected by respiratory syncytial virus. Nat. Commun. *8*, 563.
40. Galloux, M., Risso-Ballester, J., Richard, C.A., Fix, J., Rameix-Welti, M.A., and Eléouët, J.F. (2020). Minimal Elements Required for the Formation of Respiratory Syncytial Virus Cytoplasmic Inclusion Bodies In Vivo and In Vitro. mBio *11*, e01202-20.
41. Tenorio, R., Fernández de Castro, I., Knowlton, J.J., Zamora, P.F., Lee, C.H., Mainou, B.A., Dermody, T.S., and Risco, C. (2018). Reovirus σNS and μNS Proteins Remodel the Endoplasmic Reticulum to Build Replication Neo-Organelles. mBio *9*, e01253-18.
42. Fan, Y., Rao, S., Zeng, L., Ma, J., Zhou, Y., Xu, J., and Zhang, H. (2013). Identification and genomic characterization of a novel fish reovirus, Hubei grass carp disease reovirus, isolated in 2009 in China. J. Gen. Virol. *94*, 2266–2277.
43. Wei, T., Shimizu, T., Hagiwara, K., Kikuchi, A., Moriyasu, Y., Suzuki, N., Chen, H., and Omura, T. (2006). Pns12 protein of Rice dwarf virus is essential for formation of viroplasms and nucleation of viral-assembly complexes. J. Gen. Virol. *87*, 429–438.
44. Broering, T.J., Kim, J., Miller, C.L., Piggott, C.D.S., Dinoso, J.B., Nibert, M.L., and Parker, J.S.L. (2004). Reovirus nonstructural protein mu NS recruits viral core surface proteins and entering core particles to factory-like inclusions. J. Virol. *78*, 1882–1892.
45. Cai, L., Sun, X., Shao, L., and Fang, Q. (2011). Functional investigation of grass carp reovirus nonstructural protein NS80. Virol. J. *8*, 168.
46. Ahlquist, P. (2006). Parallels among positive-strand RNA viruses, reverse-transcribing viruses and double-stranded RNA viruses. Nat. Rev. Microbiol. *4*, 371–382.
47. Kopek, B.G., Perkins, G., Miller, D.J., Ellisman, M.H., and Ahlquist, P. (2007). Three-dimensional analysis of a viral RNA replication complex reveals a virus-induced mini-organelle. PLoS Biol. *5*, e220.
48. Lahaye, X., Vidy, A., Pomier, C., Obiang, L., Harper, F., Gaudin, Y., and Blondel, D. (2009). Functional characterization of Negri bodies (NBs) in rabies virus-infected cells: Evidence that NBs are sites of viral transcription and replication. J. Virol. *83*, 7948–7958.
49. Silvestri, L.S., Taraporewala, Z.F., and Patton, J.T. (2004). Rotavirus replication: plus-sense templates for double-stranded RNA synthesis are made in viroplasms. J. Virol. *78*, 7763–7774.
50. Dai, Y., Li, Y., Lin, G., Zhang, J., Jiang, N., Liu, W., Meng, Y., Zhou, Y., and Fan, Y. (2022). Non-pathogenic grass carp reovirus infection leads to both apoptosis and autophagy in a grass carp cell line. Fish Shellfish Immunol. *127*, 681–689.
51. Lin, Y.C., Boone, M., Meuris, L., Lemmens, I., Van Roy, N., Soete, A., Reumers, J., Moisse, M., Plaisance, S., Drmanac, R., et al. (2014). Genome dynamics of the human embryonic kidney 293 lineage in response to cell biology manipulations. Nat. Commun. *5*, 4767.
52. Georgi, A., Mottolahartshorn, C., Warner, A., Fields, B., and Chen, L.B. (1990). Detection of Individual Fluorescently Labeled Reovirions in Living Cells. P Natl Acad Sci USA *87*, 6579–6583.
53. Javed, A., Zaidi, S.K., Gutierrez, S.E., Lengner, C.J., Harrington, K.S., Hovhannisyan, H., Cho, B.C., Pratap, J., Pockwinse, S.M., Montecino, M., et al. (2004). In situ immunofluorescence analysis: analyzing RNA synthesis by 5-bromouridine-5′-triphosphate labeling. Methods Mol. Biol. *285*, 29–31.

STAR★METHODS

KEY RESOURCES TABLE

REAGENT or RESOURCE	SOURCE	IDENTIFIER
Antibodies		
Rabbit polyclonal anti-Flag	Proteintech	Cat#20543-1-AP; RRID:AB_11232216
Rabbit polyclonal anti-Myc	Proteintech	Cat#16286-1-AP; RRID: AB_11182162
Rabbit polyclonal anti-EGFP	Proteintech	Cat# 50430-2-AP; RRID: AB_11042881
Mouse monoclonal anti- bromodeoxyuridine (BrdU)	ABclonal	Cat#A1482; RRID: AB_2756438
Mouse monoclonal anti-β-tubulin	Proteintech	Cat#66240-1-Ig; RRID: AB_2881629
Rabbit polyclonal anti-NS38	Prepared by AtaGenix	N/A
Rabbit polyclonal anti-VP56	Gift from Jianguo Su	N/A
Rabbit polyclonal anti-VP35	Prepared by AtaGenix	N/A
HRP-conjugated Affinipure Goat Anti-Rabbit	Proteintech	Cat#SA00001-2; RRID:AB_2722564
Alexa Fluor 488 AffiniPure Goat Anti-Mouse	Yeasen	Cat# 33206ES60
Cy3-AffiniPure Goat Anti-Rabbit	ABclonal	Cat#AS007; RRID: AB_2769089
Bacterial and virus strains		
Grass Carp Reovirus(GCRV), type II, strain GCRV-AH528	Gift from Junhua Li	N/A
*trans*5α Chemically Competent Cell	TransGen Biotech	Cat#CD201-01
Chemicals, peptides, and recombinant proteins		
Bromouridine 5′-triphosphate(BrUTP)	Sigma	Cat#161848-60-8
Actinomycin D	MedChemExpress	Cat#HY-17559
Nocodazole	MedChemExpress	Cat#HY-13520
Fetal Bovine Serum (FBS)	Yeasen	Cat#40130ES76
Penicillin/Streptomycin	Gibco	Cat#15070063
Trypsin-EDTA	Gibco	Cat#R001100
TransIntro® EL Transfection Reagent	TransGen Biotech	Cat#FT201-01
Cell lysis buffer	Beyotime	Cat#P0013
4% paraformaldehyde	Biosharp	Cat#BL539A
Triton X-100	Thermoscientific	Cat#A16046.AE
Bovine serum albumin	Sigma	Cat#A9418
DAPI	Biosharp	Cat#BL105A
Nitrocellulose membranes	Biosharp	Cat#BS-NC-45
Protein A/G Magnetic Beads	MedChemExpress	Cat#HY-K0202
Anti-Flag Magnetic Beads	MedChemExpress	Cat#HY-K0207
Experimental models: Cell lines		
GCO cell(Grass carp ovary cell line)	Gift from Longfeng Lu	N/A
HEK293T cell	ATCC	CRL-3216
Oligonucleotides		
See Table S1	Tsingke Biotech	N/A
Recombinant DNA		
Plasmid pVP1-Flag	This paper	KR180368.1
Plasmid pVP2-Flag	This paper	KR180369.1

(*Continued on next page*)

Continued

REAGENT or RESOURCE	SOURCE	IDENTIFIER
Plasmid pVP3-Flag	This paper	KR180370.1
Plasmid pNS79-Flag	This paper	KR180371.1
Plasmid pVP5-Flag	This paper	KR180372.1
Plasmid pVP4-Flag	This paper	KR180373.1
Plasmid pVP56-Flag	This paper	KR180374.1
Plasmid pVP41-Flag	This paper	KR180375.1
Plasmid pVP6-Flag	This paper	KR180376.1
Plasmid pNS38-Flag	This paper	KR180377.1
Plasmid pVP35-Flag	This paper	KR180378.1
Plasmid pVP1-DsRed	This paper	KR180368.1
Plasmid pVP2-DsRed	This paper	KR180369.1
Plasmid pVP3-DsRed	This paper	KR180370.1
Plasmid pNS79-DsRed	This paper	KR180371.1
Plasmid pVP5-DsRed	This paper	KR180372.1
Plasmid pVP4-DsRed	This paper	KR180373.1
Plasmid pVP56-DsRed	This paper	KR180374.1
Plasmid pVP41-DsRed	This paper	KR180375.1
Plasmid pVP6-DsRed	This paper	KR180376.1
Plasmid pNS38-DsRed	This paper	KR180377.1
Plasmid pVP35-DsRed	This paper	KR180378.1
Plasmid pVP56-EGFP	This paper	KR180374.1
Plasmid pVP35-EGFP	This paper	KR180378.1
Plasmid pNS38-EGFP	This paper	KR180377.1
Plasmid pVP56-N-EGFP	This paper	N/A
Plasmid pVP56-M-EGFP	This paper	N/A
Plasmid pVP56-C-EGFP	This paper	N/A
Plasmid pVP35-N-EGFP	This paper	N/A
Plasmid pVP35-M-EGFP	This paper	N/A
Plasmid pVP35-C-EGFP	This paper	N/A
Plasmid pVP56-N-Myc	This paper	N/A
Plasmid pVP35-M-Myc	This paper	N/A
Software and algorithms		
NIS-Elements Viewer	Nikon	N/A
Amersham Imager 600	GE Healthcare	N/A

RESOURCE AVAILABILITY

Lead contact

Further information and requests for resources and reagents should be directed to and will be fulfilled by the lead contact, Jiagang Tu (tujiagang@mail.hzau.edu.cn).

Materials availability

This study did not generate unique reagents.

Data and code availability

All data reported in this paper will be shared by the lead contact upon reasonable request.

This paper does not report original code.

Any additional information required to reanalyze the data reported in this paper is available from the lead contact upon request.

EXPERIMENTAL MODEL AND STUDY PARTICIPANT DETAILS

Cells

Grass carp ovary (GCO) cells[50] were grown in minimum essential medium (MEM) (Gibco) containing 10% fetal bovine serum (FBS) (Gibco) and 1% penicillin/streptomycin (100 g/ml) at 28°C. 293T cells[51] were grown in Dulbecco's modified Eagle's medium (DMEM) (Gibco) containing 10% FBS (Gibco) and 1% penicillin/streptomycin (100 g/ml) at 37°C with 5% CO_2.

METHOD DETAILS

Plasmid construction

The VP1, VP2, VP3, NS79, VP5, VP4, VP56, VP41, VP6, NS38, and VP35 genes (GenBank: KR180368.1∼KR180378.1) were amplified from cDNAs of GCRV-AH528 infected GCO cells and cloned into plasmids p3XFlag-CMV-14 and pDsRed-N1. The plasmids pEGFP-VP56, pEGFP-VP35, and pEGFP-NS38 were constructed by amplifying the VP56, VP35, and NS38 genes from pFlag-VP56, pFlag-VP35, and pFlag-NS38 and cloning into plasmid pEGFP-N1. The VP56 and VP35 truncated plasmids were constructed by amplifying the truncated segments using pEGFP-VP56 and pEGFP-VP35 as templates and cloning into plasmids pEGFP-N1 and pCMV-Myc. The above required primers are shown in key resources table.

Virus infection

GCO cells at a density of 80%-90% were incubated with GCRV-AH528 for 2 h. The medium was replaced with fresh medium containing 5% FBS and incubated for the indicated times.

Immunoprecipitation (IP) and Western blotting

293T cells grown in T25 culture disk (5×10^6 cells per disk) were transfected with indicated 5 μg of plasmids using TransIntro® EL Transfection Reagent (TransGen Biotech) following the manufacturer's instructions. At 24 h post transfection, plasmid-transfected cells were collected and lysed with cell lysis buffer (Beyotime). The lysates were cleared by centrifugation at 12,000 rpm and subjected to IP using specific antibodies according to the manufacturer's instructions of protein A/G magnetic beads (MCE). The final solution was separated into 10% SDS-PAGE and transferred to 0.2 μm nitrocellulose membranes (Biosharp). Membranes were blocked for 2 h at room temperature in 5% skim milk dissolved in tris-buffered saline with 0.1% tween 20 (TBST) and incubated with the indicated primary antibodies for 2 h at room temperature. The membranes were washed three times with TBST and incubated with HRP-conjugated goat anti-rabbit antibody or anti-mouse antibody for 1 h at room temperature. The signal intensity was then determined using Amersham Imager 600 System.

Immunofluorescence and confocal microscope

For direct immunofluorescence (DIF), GCO or 293T cells were seeded on 12-mm glass coverslips (10^6 cells per coverslip). On the following day, cells were transfected with indicated plasmids. At the indicated time points, the coverslips were fixed with 4% paraformaldehyde for 20 min and counterstained with nuclear stain 4′,6-diamidino-2-phenylindole (DAPI). The samples were detected using the Nikon laser confocal microscope (100x/1.49 oil objective, Nikon, N-STORM, Japan). For indirect immunofluorescence (IIF), GCO cells were cultured on 12-mm glass coverslips overnight and then infected with GCRV-II. Cells were harvested at the indicated times. The coverslips were fixed with 4% paraformaldehyde for 20 min and permeated with 0.5% Triton X-100 for 15 min. After being blocked with 5% bovine serum albumin (BSA) for 2 h, primary antibodies diluted in 5% BSA were added and incubated at 37°C for 2 h, and then secondary antibodies diluted in 5% BSA were added and incubated at 37°C for 1 h. After each incubation step, cells were washed gently. DAPI staining was applied to detect the cell nucleus. All samples were observed using Nikon laser confocal microscope. Image acquisition and reconstruction were performed with Nikon NIS-Elements software.

Primary antibodies used were anti-GCRV-II-NS38 (1:200, rabbit polyclonal), anti-beta-tubulin (1:500, mouse monoclonal), anti-GCRV-II-VP35 (1:200, rabbit polyclonal), anti-GCRV-II-VP56 (1:200, rabbit polyclonal), and anti-BrdU (1:500, mouse monoclonal).

Secondary antibodies used in this study were Alexa Fluor 488 AffiniPure Goat Anti-Mouse IgG(H+L) antibody (1:500) and Cy3-AffiniPure Goat Anti-Rabbit IgG(H+L) antibody (1:500).

BrUTP labeling of viral RNAs

To locate the viral RNAs, a uridine analog, bromouridine 5′-triphosphate (BrUTP) (Sigma-Aldrich) that could be incorporated into RNA during its synthesis,[52,53] was used to label viral RNAs. In detail, GCRV-II-infected GCO cells at 15 h post infection (hpi) were treated with 10 μg/ml Actinomycin D (ActD, MCE) for 30 min and then transfected with BrUTP (Sigma) at a final concentration of 10 mM by using TransIntro® EL Transfection Reagent (TransGen Biotech) and then incubated in the presence of ActD for 1 h. The cells were fixed and permeabilized as described above and processed for indirect immunofluorescence.

QUANTIFICATION AND STATISTICAL ANALYSIS

Three independent experimental replicates were performed for all experiments unless otherwise stated.